Kagome Compounds

Xiaolong Feng[#], Subhajit Roychowdhury[##], ErJian Cheng, ChangJiang Yi, Dong Chen and Claudia Felser[###]

Kagome lattices host interesting electronic states, including Dirac points, van Hove singularities, and flat bands, at varied fillings. Furthermore, the interplay between the charge order, electronic correlation, and topology results in exotic physical properties, such as unconventional charge density waves in AV_3Sb_5, large anomalous Hall effects in $LiMn_6Sn_6$, and large thermoelectric effects in YMn_6Sn_6. Recently, ScV_6Sn_6 was reported to exhibit charge density waves with a different vector than those in AV_3Sb_5. In contrast to the enhanced superconductivity in AV_3Sb_5 under external pressure, no superconductivity is observed in ScV_6Sn_6, except for suppressed charge density waves, even though both compounds present van Hove singularities close to the Fermi level. Through high-throughput first-principles calculations, we identified a range of phonon instabilities and electronic flat bands in ScV_6Sn_6-type kagome compounds. Our predictions suggest a vast kagome family with rich properties induced by flat bands, van Hove singularities, and their interplay with electronic correlations.

The interaction between geometry, topology, and correlation gives rise to abundant properties in condensed matter. One unique geometry is the kagome lattice of corner-sharing triangles. Electrons in kagome lattices exhibit various intriguing electronic states at different fillings, including flat bands, van Hove singularities (vHSs), and Dirac points. While the Dirac point presents nontrivial topological properties, the flat bands and vHSs show a distinct density of states (DOS) and electron susceptibility, indicating enhanced electron–electron correlation and potential for Stoner flat bands/Fermi surface instability. Materials with kagome lattices exhibit a range of fascinating properties [1-3], including charge density waves (CDWs), quantum spin liquids, and unconventional superconductivity. A recent example is the AV_3Sb_5 (A = K, Rb, or Cs) kagome superconductor, which hosts vHSs near the Fermi level and unconventional CDWs. Superconductivity is also observed below the CDW transition temperature. Under external pressure, the superconductivity is significantly enhanced, whereas the CDWs are suppressed. Similarly to AV_3Sb_5, ScV_6Sn_6 also exhibits vHSs near the Fermi level and a CDW transition in a distinct vector [4–6]. However, unlike AV_3Sb_5, no superconductivity is observed. Gaining a deeper understanding of these fundamental mechanisms is becoming increasingly important in this field.

Charge density waves driven by electron–phonon coupling in ScV_6Sn_6

ScV_6Sn_6 crystallizes in a hexagonal centrosymmetric structure (space group *P*6/*mmm*, No. 191) at room temperature, with the V atoms forming a kagome lattice in the *ab* plane (Figure 1a). Temperature-dependent magnetization and electrical resistivity measurements indicate a sharp CDW transition at 92 K, characterized by a first-order transition with propagation vector (1/3, 1/3, 1/3). The zero-field electrical resistivity displays metallic behavior, with a significant drop at the CDW transition temperature owing to softening of the acoustic phonon modes; thus, ScV_6Sn_6 shows unconventional out-of-plane lattice dynamics.

The distinct CDW in ScV_6Sn_6 raises an intriguing question about its origin. In contrast to the 2 × 2 × 2 modulation in AV_3Sb_5, ScV_6Sn_6 exhibits a CDW with a modulation vector at (1/3, 1/3, 1/3). However, the inelastic X-ray spectrum suggests that phonon softening occurs at (1/3, 1/3, 1/2) (Figure 1b), with good agreement to the calculated phonon spectrum [4]. Angle-re-

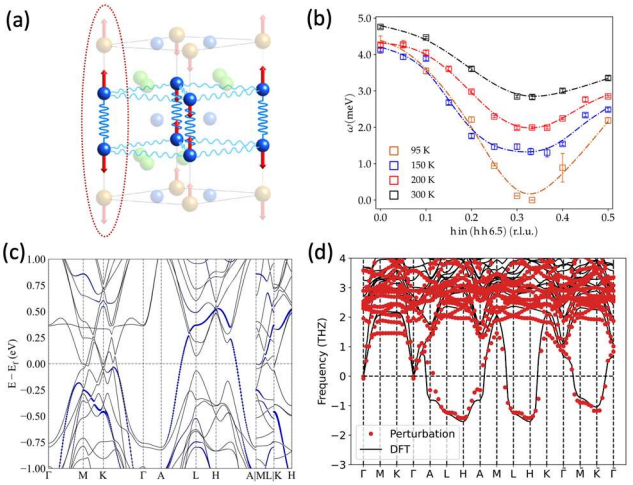

Fig. 1: (a) Z-direction vibration of trigonal Sn atoms in ScV_6Sn_6. (b) Phonon frequency obtained from inelastic X-ray scattering at various temperatures, displaying phonon softening at (1/3, 1/3, 1/2) above the charge density wave transition temperature. (c) Band structure of pristine phase, weighted by Sn p_z orbitals. (d) Phonon spectrum from density functional theory calculations at low temperature and model based on perturbation theory, suggesting electron–phonon coupling.

solved photoemission spectroscopy and density functional theory (DFT) calculations also revealed that the CDW gap in the bands is dominated by Sn p_z orbitals (Figure 1c). Based on the physical Gaussian approximation and perturbation theory, a weakly coupled one-dimensional Sn–Sn chain model was proposed to interpret the phonon softening at (1/3, 1/3, 1/2). The model matched the DFT calculations well (Figure 1d), indicating that the coupling between the phonon mode of the out-of-plane vibration of the trigonal Sn atoms and their p_z orbitals drives phonon softening. These results show the distinct origin of the CDW in ScV_6Sn_6.

Topological band revealed by Quantum Oscillation

At low temperatures, ScV_6Sn_6 exhibits Shubnikov–de Haas (SdH) quantum oscillations in the transverse resistivity, which help in mapping the Fermi surface topology (Figure 2). These oscillations, starting from approximately 1.5 T at 2 K, indicate the existence of small Fermi surface pockets along with a large Fermi surface (Figure 2a and 2b). The fast Fourier transform (FFT) of these oscillations reveals three distinct frequencies (F_α = 10 T, F_β = 28 T, and F_γ = 50 T) of small Fermi surfaces (Figure 2c). We estimated the effective masses of charge carriers corresponding to these Fermi surface pockets using the Lifshitz–Kosevich theory. The analysis revealed a nontrivial Berry phase from the Landau fan diagram, confirming the nontrivial topological Fermi surface.

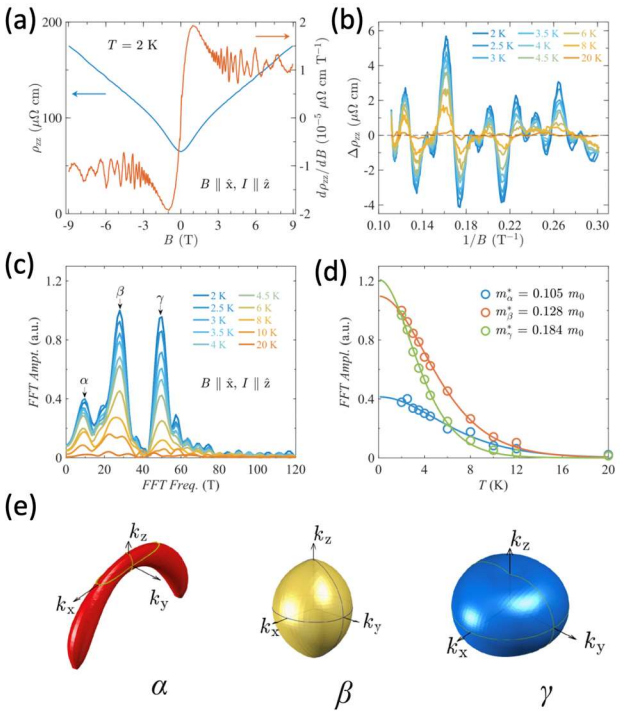

Fig. 2: (a) Longitudinal ρ_{zz} of ScV_6Sn_6 at 2 K and its first derivative with field showing quantum oscillations. (b) Background-subtracted Shubnikov–de Haas oscillation amplitude at several temperatures. (c) Corresponding fast Fourier transform (FFT) amplitude exhibiting α, β, and γ frequencies. (d) FFT amplitude fitting of effective mass. (e) Theoretically calculated 3D Fermi surfaces.

Interestingly, ScV_6Sn_6 also exhibits anomalous Hall-like behavior below the CDW transition temperature, suggesting the possible breaking of the time-reversal symmetry. Our research demonstrates that ScV_6Sn_6, as a member of the versatile MT_6Z_6 (166) family, presents unique opportunities for exploring the interplay between kagome lattice structures and CDW transitions, contributing significantly to our understanding of topological materials and their associated quantum phenomena.

Intrinsic anomalous Hall effect

One interesting topic is the intrinsic anomalous Hall effect derived from the nontrivial band topology. $LiMn_6Sn_6$, another member of the 166 family, is notable for its ferromagnetism with a high Curie temperature of 382 K and easy plane along the kagome lattice (Figure 3a). At low temperatures, the magnetoresistance of $LiMn_6Sn_6$ is positive and does not saturate below 9 T, indicating the presence of mechanisms other than spin-disorder scattering. Hall resistivity measurements showed opposite signs for the ordinary Hall coefficients for ρ_{xz} and ρ_{yx}, suggesting the coexist-

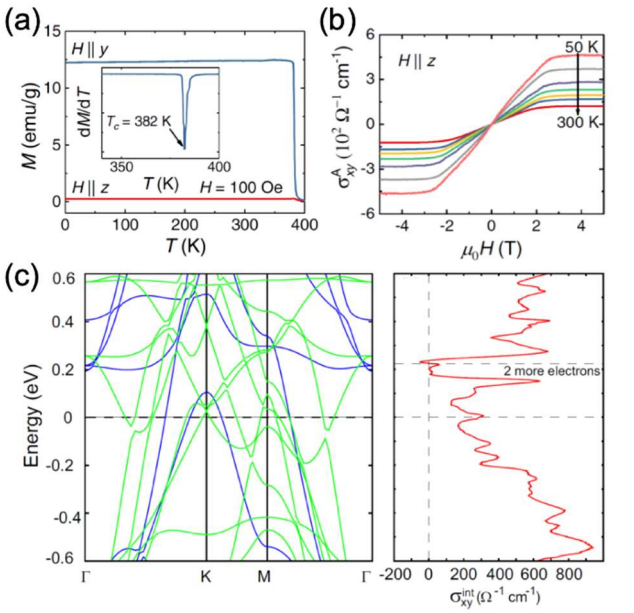

Fig. 3: (a) Temperature dependence of magnetization of $LiMn_6Sn_6$ under magnetic field H = 100 Oe. Inset: Derivative of magnetization dM/dT vs. T for H||y. (b) Anomalous Hall conductivity (AHC) with H||z at various temperatures. (c) Band structure of $LiMn_6Sn_6$ and energy dependence of intrinsic AHC.

ence of electron and hole carriers. Moreover, a significant intrinsic contribution to the anomalous Hall conductivity (AHC) of 380 Ω^{-1} cm^{-1}, or 0.44 e^2 h^{-1} per Mn layer, was observed, which is significantly higher than those observed in other RMn$_6$Sn$_6$ compounds (R = rare earth element(s)) (Figure 3b).

This large anomalous Hall effect is attributed to band crossings near the Fermi energy, including a spin-polarized Dirac point at the K point (Figure 3c). The intrinsic AHC calculated from the Berry curvature also peaked near the Fermi energy, which aligns closely with experimental observations. These findings contribute to a broader understanding of anomalous Hall effects in magnetic materials and open avenues for further research into kagome materials and their applications in spintronics.

Large anomalous transverse thermoelectric effect

Conventional thermoelectric devices, which rely on the Seebeck effect, have several drawbacks, such as the need for *p*- and *n*-type materials and complex electrical connections. In contrast, transverse thermoelectric devices based on the Nernst effect offer a simpler single-material solution. YMn$_6$Sn$_6$ is of particular interest because it crystallizes into a hexagonal structure, with the Mn atoms forming a kagome lattice. It exhibits a high Néel temperature of approximately 340 K, making it suitable for room-temperature applications (Figure 4a).

The antiferromagnetic (AFM) structure of YMn$_6$Sn$_6$ avoids stray magnetic fields typical of ferromagnetic (FM) materials, thus reducing interference with other devices. YMn$_6$Sn$_6$ exhibits a large anomalous Nernst effect (ANE) of ~2 μV K^{-1} at 300 K, which is higher than that of other canted AFM materials and comparable to FM systems (Figure 2b). This large ANE was attributed to the intrinsic Berry curvature near the Fermi level (Figure 2c). Additionally, the Seebeck coefficient of YMn$_6$Sn$_6$ shows a strong dependence on the magnetic field, which is related to the substantial release of entropy during the magnetic structural transition. Our findings suggest that AFM materials with high magnetic transition temperatures and significant Berry curvatures exhibit superior performance in room-temperature thermoelectric applications.

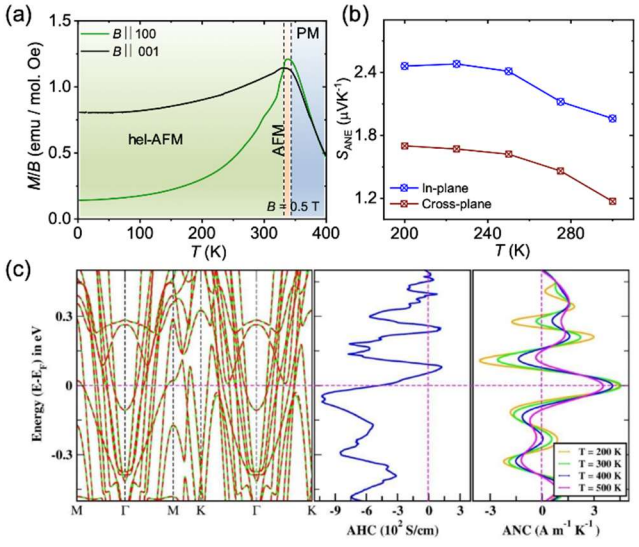

Fig. 4: (a) Temperature-dependent field-cooled (FC) magnetic susceptibility of YMn$_6$Sn$_6$ at B = 0.5 T for B||100 and B||001, showing the antiferromagnetic (AFM), helical antiferromagnetic (hel-AFM), and paramagnetic (PM) regions. (c) Band structure of YMn$_6$Sn$_6$ (left) and theoretical anomalous Hall and Nernst conductivities (AHC and ANC, respectively) (right) as a function of Fermi energy.

Prediction of novel MT_6Z_6 bilayer kagome compounds

A recent high-throughput DFT calculation of 293 MT_6Z_6 bilayer Kagome compounds with HfFe$_6$Ge$_6$-type structures (space group *P6/mmm*; No. 191), including their electronic band structures and phonon spectra, found 166 to be stable. The remaining structures presented imaginary phonon instabilities, providing insight into potential structural phase transitions.

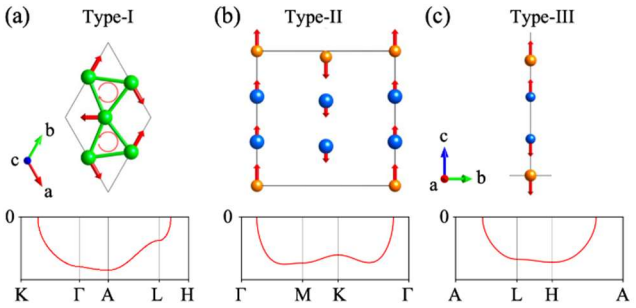

Fig. 5: Dominant vibration modes with corresponding imaginary instabilities in MT_6Z_6 kagome compounds. (a) Type-I instabilities occurring along the Γ–A path are primarily characterized by in-plane vibrations of kagome T atoms. (b) Type-II instabilities, which occur on the k_z = 0 plane, are dominated by out-of-plane vibrations in the M–Z chains of NiIn-166. The displacements illustrate the out-of-plane movements of M and Z atoms in the same direction within the M–Z chains, but in the opposite direction in neighbor chains. (c) Type-III instabilities, observed on the $k_z = \pi$ plane, are dominated by out-of-plane vibrations in the M–Z chains of VGe/VSn/NbSn-166.

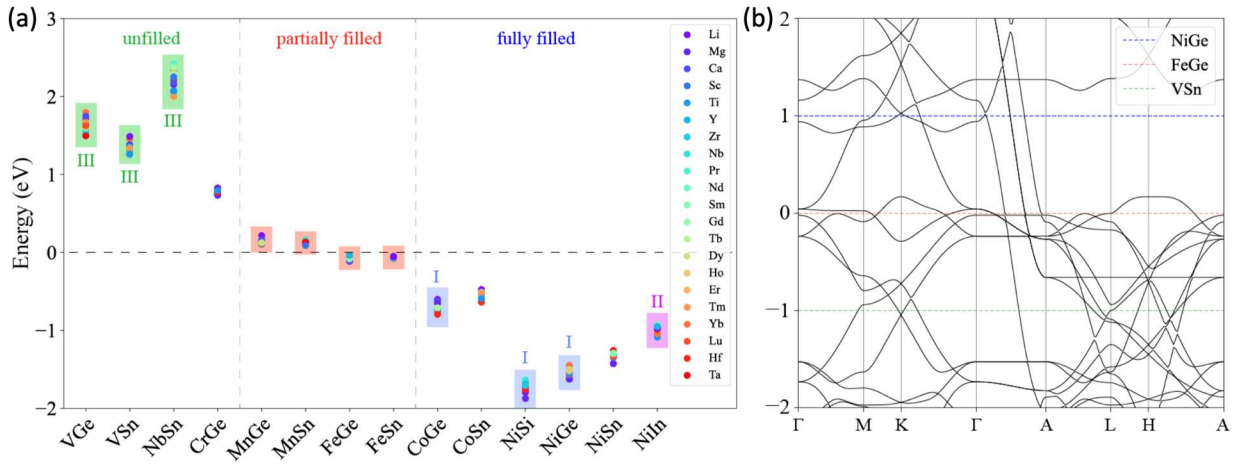

Fig. 6: Flat bands in MT_6Z_6 kagome compounds. (a) Density of states (DOS) peaks obtained from non-spin-polarized calculations without SOC. The flat bands that contribute to the DOS can be classified into three classes: unfilled, partially filled, and fully filled. (b) Band structure from minimal tight-binding model for FeGe, where the two quasi-flat bands near the Fermi level are contributed by $d_{xy/x2-y2}$ and $d_{xz/yz}$ of Fe. The approximated Fermi levels of VSn, FeGe, and NiGe families are illustrated to present the unfilled, partially filled, and fully filled flat bands.

Potential CDWs in MT_6Z_6 compounds

Except for Mn/Fe-based kagome structures, the instabilities in other MT_6Z_6 compounds are categorized into three classes based on their imaginary modes. Type-I instabilities occur in the CoGe/NiSi/NiGe family, in which the leading instabilities occur along the Γ–A path, governed by in-plane distortions within the kagome networks. Type-II instabilities, which have been observed in the NiIn family, contain nearly flat imaginary modes on the $k_z = 0$ plane, which exhibits out-of-plane movements in the same direction within the *M*–*Z* chains, whereas the direction may alternate in neighboring chains. Type-III instabilities, which are found in the VGe/VSn/NbSn family, contain a nearly flat imaginary mode on the $k_z = \pi$ plane. In contrast to the movements in the same direction within each chain, type-III instabilities exhibit opposite movements of *M* and *Z* atoms within each chain. One notable example of materials with type-III instability is ScV_6Sn_6, which exhibits competing charge orders at low temperatures [4-6].

Flat bands in kagome compounds

MT_6Z_6 kagome compounds share similar band structures despite having different electron fillings. The electronic features at the Fermi level are dominated by kagome-derived bands from the *T* elements. Hence, the electron filling is primarily determined by the number of valence electrons and is further modified by the *Z* and *T* atoms. In MT_6Z_6 compounds, the kagome T atoms are mainly occupied by 3*d* elements and 4*d* Nb. Furthermore, in the MT_6Z_6 environment, the five *d* orbitals are split into three groups: in-plane $d_{xy/x2-y2}$ and out-of-plane $d_{xz/yz}$ and d_{z2} orbitals. The coupling between the *d* orbitals of the kagome *T* atoms and *p* orbitals of the *Z* atoms contributes to the complicated band structure.

Notably, the flat bands from $d_{xy/x2-y2}$ and $d_{xz/yz}$ have similar energies, contributing to the largest DOS peak, whereas the d_{z2} orbital contributes to a minor DOS peak. The locations of the DOS peaks are mainly determined by *T* and *Z*, particularly the transition element *T* at the kagome sites. When the *d* orbitals are nearly half-filled, flat bands emerge near the Fermi level with a sharp DOS peak, indicating possible instabilities of the Fermi surface and enhanced correlations. This is the case for Mn($3d^5$)-166 and Fe($3d^6$)-166, in which magnetic ordering has been extensively reported. In V/Nb/Cr-166, there are fewer valence *d* electrons, which lifts the flat bands above the Fermi level. By contrast, Co/Ni-166 has more valence *d* electrons, which pushes the flat bands below the Fermi level.

Importantly, the electronic properties of MT_6Z_6 bilayer kagome compounds can be interpreted from their parent *TZ* structure. The intercalation of *M* atoms can be understood as a perturbation that pushes the trigonal *Z* atoms away from the Kagome plane, resulting in a doubling along the *c* direction. Therefore, the corresponding Brillouin zone is folded, intertwining the Kagome-derived bands while preserving the main features.

Flat-band-driven magnetism

The Mn/Fe-166 compounds exhibited pronounced DOS peaks near the Fermi level because of the half-filling of the 3*d* elements at the kagome sites, indicating possible instability at low temperatures. This has been confirmed by non-spin-polarized calculations. Experimentally, all existing Mn/Fe-166 materials exhibit strong magnetic orders, and most of them tend to form AFM orders with FM intralayer interactions but AFM interlayer interactions. By contrast, Mn-166 compounds exhibit more diverse magnetic structures. By estimating the filling of the flat bands, it can be observed that when the filling approaches half, some Mn-166 compounds, such as M = Zr and Hf, exhibit AFM orders. At lower fillings (<0.2), other Mn-166 compounds, such as M = Li and Mg, prefer FM orders. Interestingly, for each Mn/Fe-166 class, a higher magnetic transition temperature is observed when the filling approaches half. With the inclusion of magnetic orders, additional calculations show splitting of the DOS and elimination of phonon instabilities. Note that a CDW transition is still observed in FeGe without imaginary phonons in the presence of vHSs near the Fermi level, indicating an interplay between the spin, phonons, vHSs, and CDWs in related systems.

CDW in magnetic kagome compounds

Given that the phonon instabilities found in Fe/Mn kagome compounds stem from flat bands in proximity to the Fermi level in PM phases, the introduction of magnetic order eradicates all phonon instabilities. One may wonder whether CDW transitions would occur in magnetic kagome compounds. A recent notable example is FeGe, which exhibits CDW transitions in the AFM phase, coinciding with an increase in magnetic moment, without any phonon instabilities. Theoretical models suggest spin–phonon coupling as a possible origin.

Recently, the Kagome family LnTi$_3$Bi$_4$ has also garnered significant interest due to its composition of four distorted Kagome layers and zigzag chains. Similar to other Kagome compounds mentioned earlier, the electronic characteristics of LnTi$_3$Bi$_4$ close to the Fermi level are primarily governed by the Ti kagome networks, featuring Dirac points and vHSs. In TbTi$_3$Bi$_4$, the Tb atoms form the zigzag chains, which display AFM behavior below 20.4 K [7]. Notably, when a magnetic field is applied along the zigzag chain direction, plateaus at 1/3 and 2/3 of the saturated magnetization are observed. Furthermore, ARPES measurements reveal band folding and gap opening below the

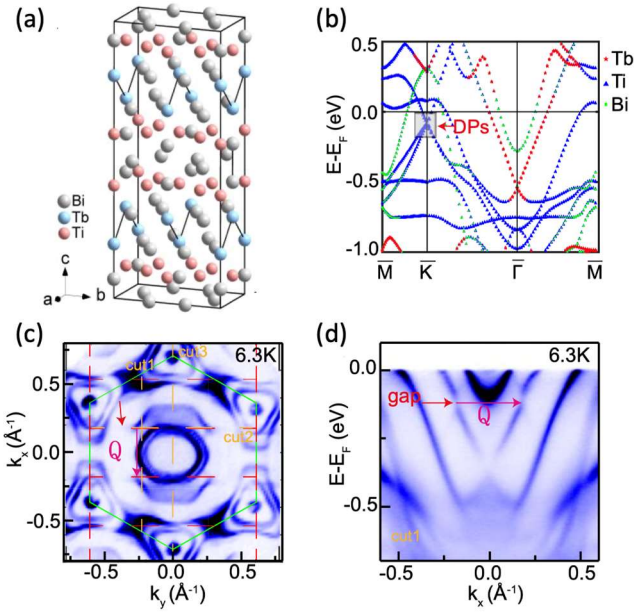

Fig. 7: CDW in kagome compound TbTi$_3$Bi$_4$. (a) Crystal structure of TbTi$_3$Bi$_4$, composed of distorted Ti kagome nets and Tb zigzag chains. (b) Band structure with the atomic projections. The electronic properties is dominated by the Ti kagome nets, featured by Dirac points and vHSs closed to the Fermi level. (c) The energy contour at the Fermi level by ARPES measurements. (d) Band dispersion along the dashed orange cut, which reveals a significant CDW gap near the Fermi level.

transition, indicating the strong coupling between magnetism and the spin/charge density wave. The band folding corresponds to a vector q = (1/3, 0, 0). However, current STM results haven't confirmed the presence of charge modulation, which requires further investigation into the cause of the band folding and gap opening.

Outlook

Kagome-derived bands present Dirac points, vHSs, and flat bands at different fillings. Element substitutions can give rise to large compound diversity, in which Kagome features can be found near the Fermi levels. However, similar fillings may still reveal distinct properties, as observed for ScV$_6$Sn$_6$ and AV$_3$Sb$_5$. In AV$_3$Sb$_5$ the CDW transition is more likely to be caused by Fermi surface nesting, while electron–phonon coupling plays a more important role in the CDW transition in ScV$_6$Sn$_6$. Under external pressure, in contrast to the competition between superconductivity and CDWs in AV$_3$Sb$_5$, no superconductivity is observed in ScV$_6$Sn$_6$ up to 11 GPa. It is important to highlight that the band structures undergo changes when subjected to pressure. In AV$_3$Sb$_5$ vHSs are pushed away from the

Fermi level whereas in ScV_6Sn_6 they shift towards the Fermi level. Their unique variations in band evolution may contribute to their distinct behaviors under pressure. Interestingly, recent experiments have reported the competition of CDW and superconductivity in $CsCr_3Sb_5$ under pressure, although it behaves as a bad metal at ambient pressure, characterized by electron correlation and frustrated magnetism. Meanwhile, flat bands from Cr kagome networks are found near the Fermi level, instead of vHSs. In addition, multiple charge orders have also been reported for the kagome superconductor $LaRu_3Si_2$, and the electronic features at the Fermi level still remain to be elucidated. Besides the perfect kagome compounds, interesting properties have also been observed in "breathing" kagome lattices, such as spin ice state in HoAgGe. With the interplay of superconductivity, charge orders, and correlation, kagome compounds with varying fillings provide a fascinating space for exploring the properties of kagome bands.

References

[1]* *Large anomalous Hall effect in the kagome ferromagnet $LiMn_6Sn_6$, D. Chen, C. Le, C. Fu, H. Lin, W. Schnelle, Y. Sun, C. Felser, Phys Rev B **103** (2021) 144410,* https://doi.org/10.1103/PhysRevB.103.144410

[2]* *Anomalous thermoelectric effects and quantum oscillations in the Kagome metal CsV_3Sb_5, D. Chen, B. He, M. Yao, H. Lin, W. Schnelle, Y. Sun, J. Gooth, L. Taillefer, C. Felser, Phys Rev B **105**, (2022) L201109,* https://doi.org/10.1103/PhysRevB.105.L201109

[3]* *Large room temperature anomalous transverse thermoelectric effect in kagome antiferromagnet YMn_6Sn_6, S. Roychowdhury, A. M. Ochs, S. N. Guin, K. Samanta, J. Noky, C. Shekhar, M. G. Vergniory, J. E. Goldberger, C. Felser, Adv Mater **34**, (2022) 2201350,* https://doi.org/10.1002/adma.202201350

[4]* *Softening of a flat phonon mode in the kagome ScV_6Sn_6, A. Korshunov, H. Hu, D. Subires, Y. Jiang, D. Călugăru, X. Feng, A. Rajapitamahuni, C. Yi, S. Roychowdhury, M. G. Vergniory, J. Strempfer, C. Shekhar, E. Vescovo, D. Chernyshov, A. H. Said, A. Bosak, C. Felser, B. A. Bernevig, S. Blanco-Canosa, Nat Commun **14** (2023) 6646,* https://doi.org/10.1038/s41467-023-42186-6

[5]* *Quantum oscillations revealing topological band in kagome metal ScV_6Sn_6, C. Yi, X. Feng, N. Mao, P. Yanda, S. Roychowdhury, Y. Zhang, C. Felser, C. Shekhar, Phys Rev B **109** (2024) 035124,* https://doi.org/10.1103/PhysRevB.109.035124

[6]* *Tuning charge density wave of kagome metal ScV_6Sn_6, C. Yi, X. Feng, N. Kumar, C. Felser, C. Shekhar, New J Phys **26** (2024) 052001,* https://doi.org/10.1088/1367-2630/ad4389

[7]* *Giant anomalous Hall effect and band folding in a Kagome metal with mixed dimensionality, E. Cheng, K. Wang, S. Nie, T. Ying, Z. Li, Y. Li, Y. Xu, H. Chen, R. Koban, H. Borrmann, W. Schnelle, V. Hasse, M. Wang, Y. Chen, Z. Liu, C. Felser, arXiv:2405.16831 (2024),* https://doi.org/10.48550/arXiv.2405.16831

[#] xiaolong.feng@cpfs.mpg.de
[##] subhajit.roychowdhury@cpfs.mpg.de
[###] claudia.felser@cpfs.mpg.de